Characterizing the Optical Fingerprint of Duodenal Gastrinoma Using Quantitative Multi-Photon Autofluorescence Microscopy

Thomas G. Knapp[1], Suzann Duan[2], Juanita L. Merchant[2], Travis W. Sawyer[1,2,3]

Department of Biomedical Engineering,[1] College of Medicine,[2] and College of Optical Sciences,[3] University of Arizona

Background and Aim(s)

Duodenal gastrinomas (DGASTs) are a type of gastroenteropancreatic neuroendocrine tumor (NET) that produce the hormone gastrin. Secretion of the hormone gastrin from **DGASTs** can lead to the development of **Zollinger-Ellison Syndrome (ZES)** which is tied to the overproduction of stomach acid. Symptoms of **ZES** includes chronic diarrhea, stomach ulcers, tissue adhesions with increased risk of rupture, and malabsorption. **DGASTs** typically develop as small, diffuse, lesions within the submucosa of the proximal small intestine. [1]
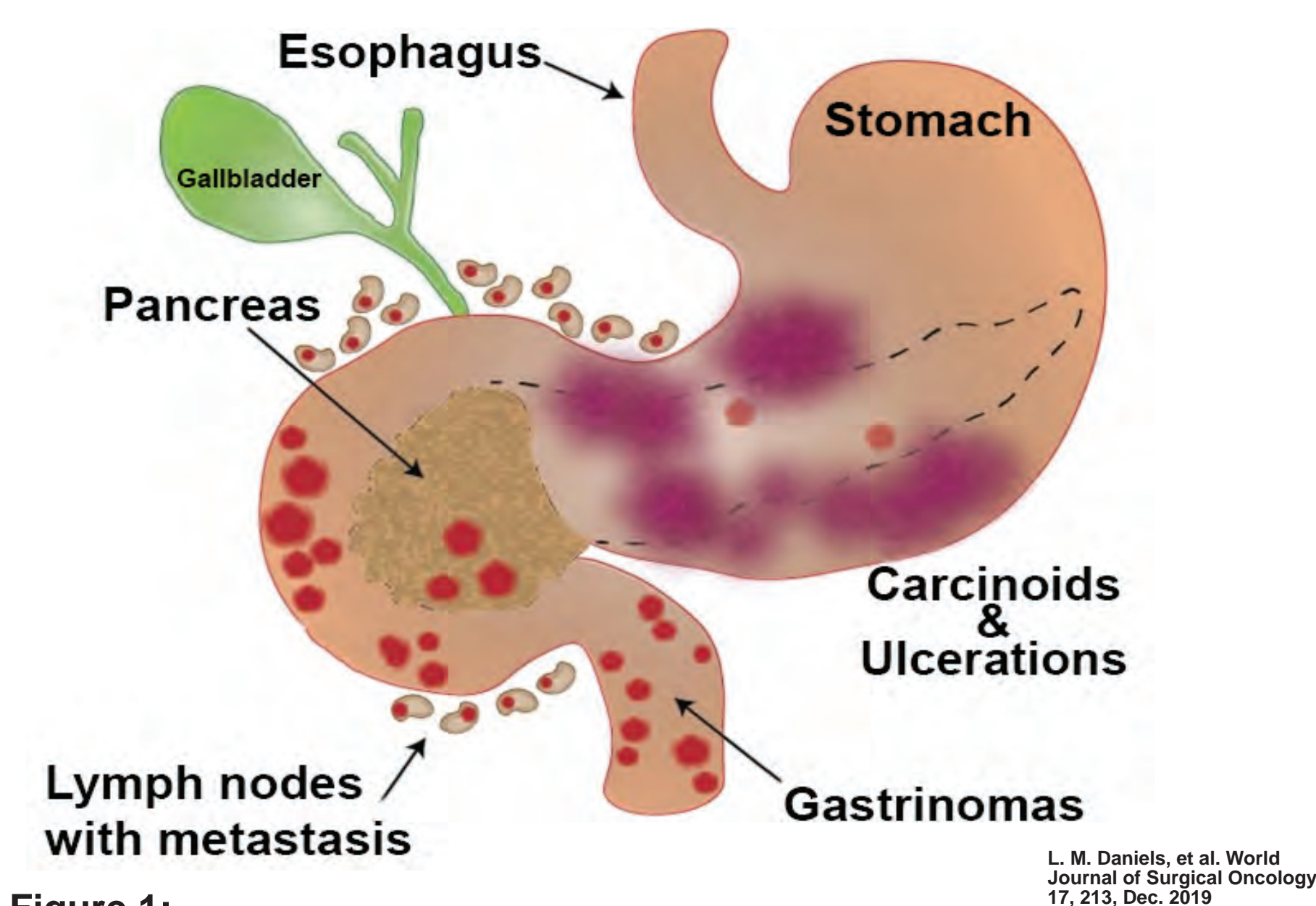

Figure 1:
Illustration of gastrinoma development and spread, showing the multifocal nature of the tumor and gastric damage secondary to acid hypersecretion.

L. M. Daniels, et al. World Journal of Surgical Oncology 17, 213, Dec. 2019

Endoscopic resection of duodenal NETs is an increasingly popular means of treating this disease but suffers from discrepancies between endoscopically and pathologically complete resections which has been shown to increase the likelihood of NET recurrence. [2]

	EMR (n=18)	EMR-L (n=16)	EMR-P (n=3)	ESD (n=4)
Mean procedure time (range, min)	13 (4-39)	14 (10-35)	18 (12-26)	33 (12-48) *
Mean resection size (range, mm)	7 (2-18)	7 (5-12)	12 (8-17) *	12 (10-5) *
Mean lesion size (range, mm)	6 (2-12)	5 (2-8)	6 (3-8)	6 (4-9)
Endoscopic complete resection	16 (89%)	16 (100%)	3 (100%)	4 (100%)
Pathological complete resection	10 (56%)	4 (25%)	1 (33%)	4 (100%) **
Bleeding	1 (6%)	0 (0%)	1 (33%)	3 (75%) ***

* = P < 0.05, ** = P < 0.01, *** = P < 0.001
Adapted from: Kim, G.H & Research, T.K.C. of H. and U.G. (2014).
Endoscopic resection for duodenal carcinoid tumors: A multicenter, retrospective study.
Journal of Gastroenterology and Hepatology, 29(2), 318–324. https://doi.org/https://doi.org/10.1111/jgh.12390

Figure 2:
Comparison of outcomes between endoscopic mucosal resection (EMR), EMR with ligation device (EMR-L), EMR with precutting (EMR-P) and endoscopic submucosal dissection (ESD) for duodenal carcinoid tumors. Endoscopically clear resection = negative margins during endoscopic procedure. Pathologically clear resection = negative margins during pathology assessment.

Hypothesis

Differences in the abundance of endogenous fluorophores in DGASTs and normal duodenal tissue will result in inherent autofluorescent contrasts measurable with multiphoton microscopy, providing a method for performing label-free *in vivo* tumor analysis.

Methods

Endogenous fluorescence was measured in formalin-fixed paraffin-embedded (FFPE) **DGast** samples from 12 patients using two-photon microscopy (Zeiss LSM 880 NLO microscope).† Excitation wavelengths and detection bands (**Figure 3**) were chosen to acquire two-photon excited fluorescence (2PEF) predominantly from **NADH**, **FAD**, **porphyrin**, and **lipofuscin** fluorophores that have abundances related to common markers of cancer. [3, 4]

Second-harmonic generation (SHG) is a light-scattering phenomena that is elicited by anti-centrosymmetric structures such as collagen. **SHG** was measured with an 880 nm excitation and 430 - 450 nm detection band.

Figure 3:
Fluorescence spectra of endogenous fluorophores used for image contrast in this study. Note, fluorescence emission occurs at varying excitation light wavelengths, allowing for overlapping detection bands without severe fluorescence crosstalk.

Croce et al.
European Journal of Histochemistry, 22 Oct. 2014, DOI:10.4081/ejh.2014.2461

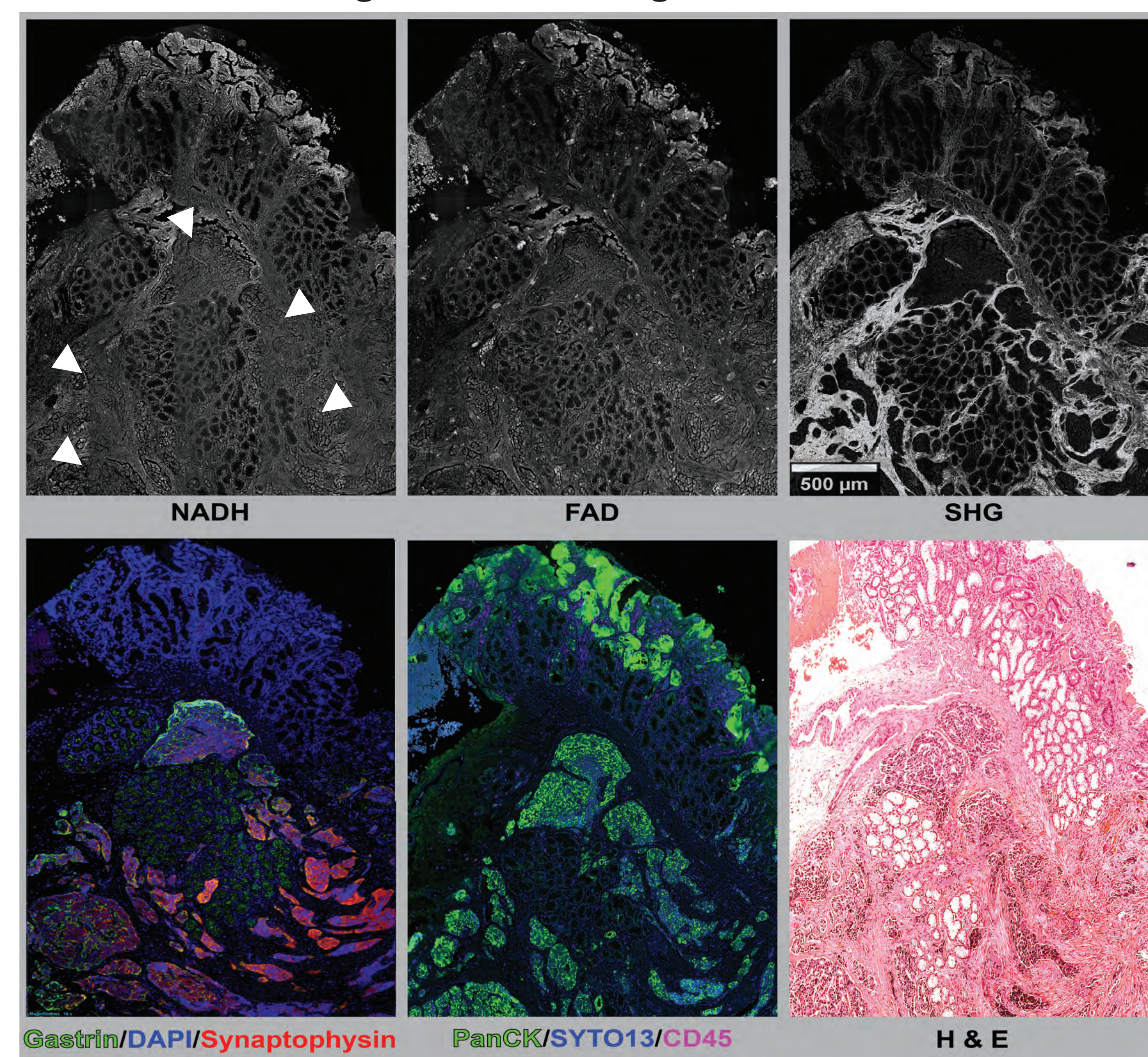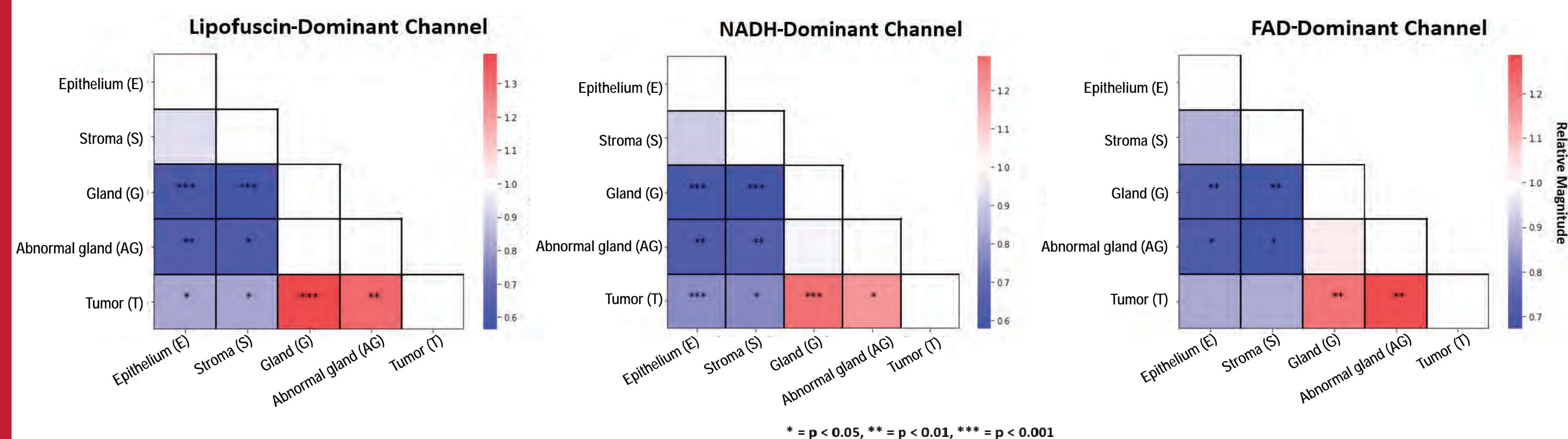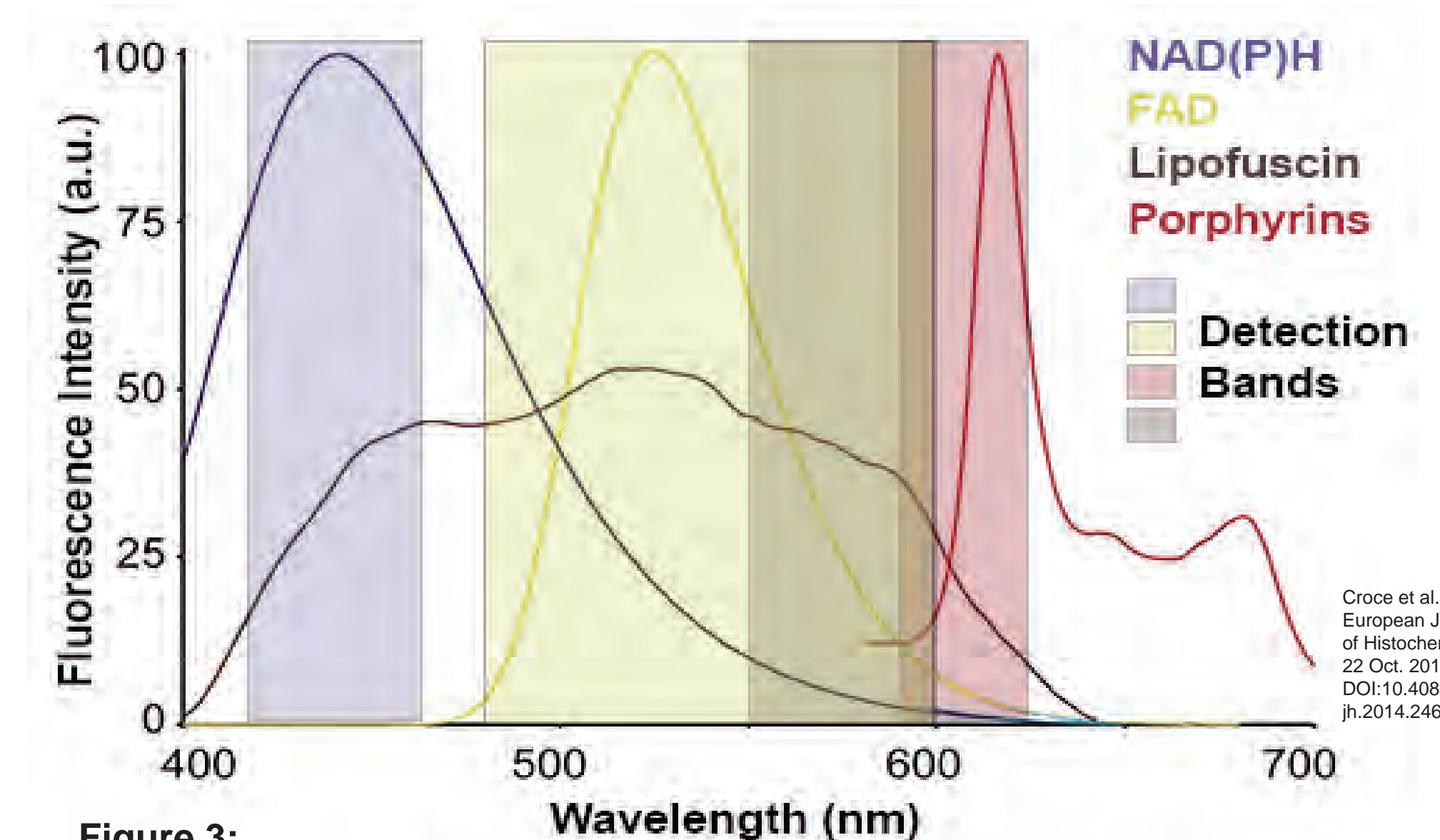### Multiphoton microscopy and immunostained images of duodenal gastrinoma

Figure 4:
Comparison of three of the imaging channels captured with two-photon microscopy (top row) and three different types of staining used to validate tissue types. Immunostaining for gastrin, a marker of gastrin-expressing cells and synaptophysin, a merker of NETs. PanCK/SYTO13/CD45 are specific for epithelium, DNA, and immune cells, respectively. Diffuse tumor regions are marked with white arrowheads.

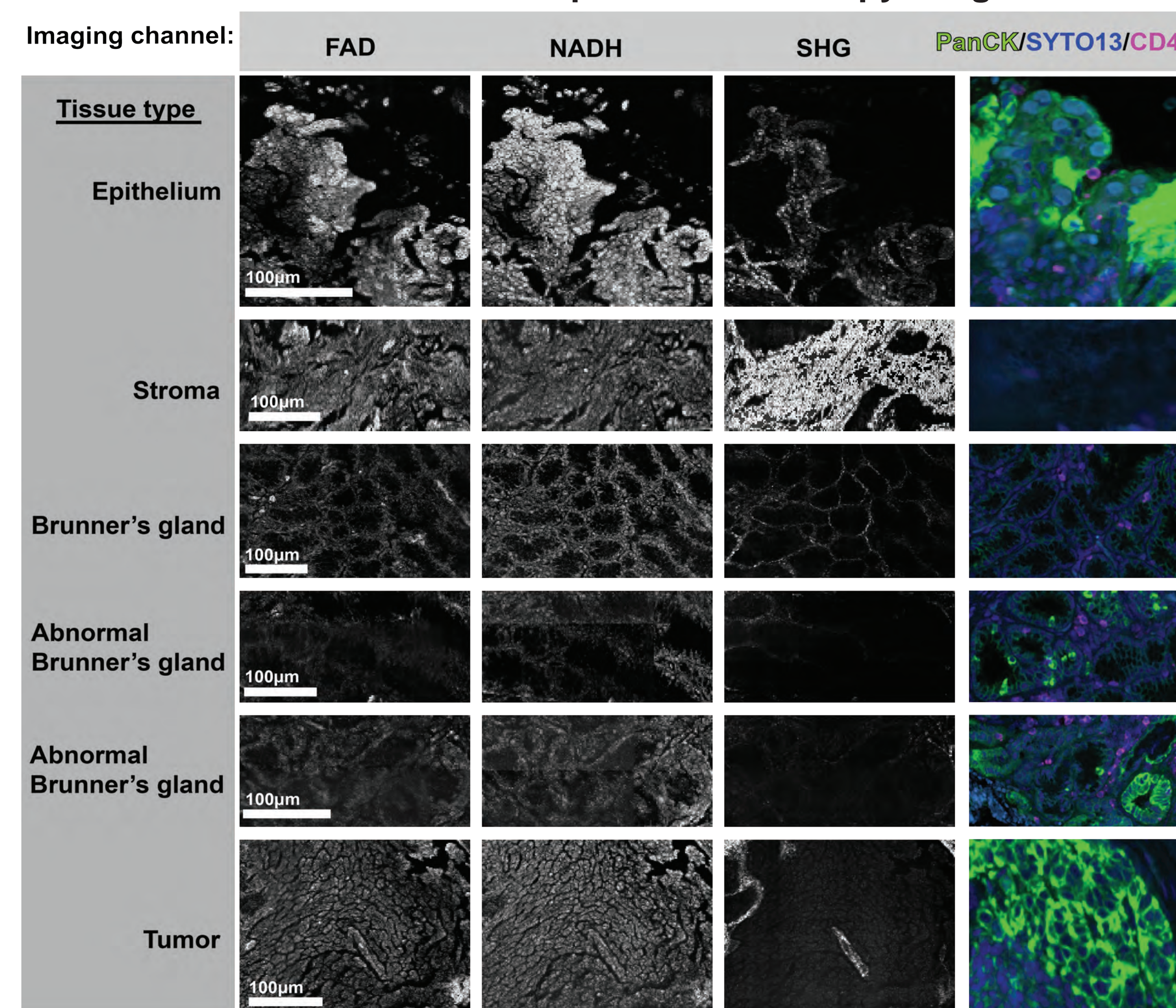### Regions of interest (ROIs) isolating tissue types within multiphoton microscopy images

Figure 5:
ROIs of different tissue classes used to measure and compare relative signal magnitudes from the 2PEF and SHG image channels. Notable morphologic changes occur between the normal/abnormal Brunner's glands and tumors, such as the degree of stromal thickening and disorganization. Notably, the defined collagen structure within the gland tissue seen in SHG imaging is diminished in the abnormal glands. The immunostaining images (shown on far right) were used to distinguish between sites of normal/abnormal glands, where abnormal glands expressed PanCK and stained positively for gastrin.

Results

Figure 6:
Heat matrices showing results of paired t-tests for the magnitude of 2PEF between tissue classes. Matrices are intrepreted by **dividing the row by the column**. The significant difference in the magnitude of endogenous fluorescence between tumor and normal tissue provides a label-free (not requiring fluorescent dyes) optical contrast. ROIs were thresholded to limit cross-talk between image channels and background noise. Comparisons between the tissue classes were made only from within-sample ROIs to control for variations in acquisitions and samples.

* = p < 0.05, ** = p < 0.01, *** = p < 0.001
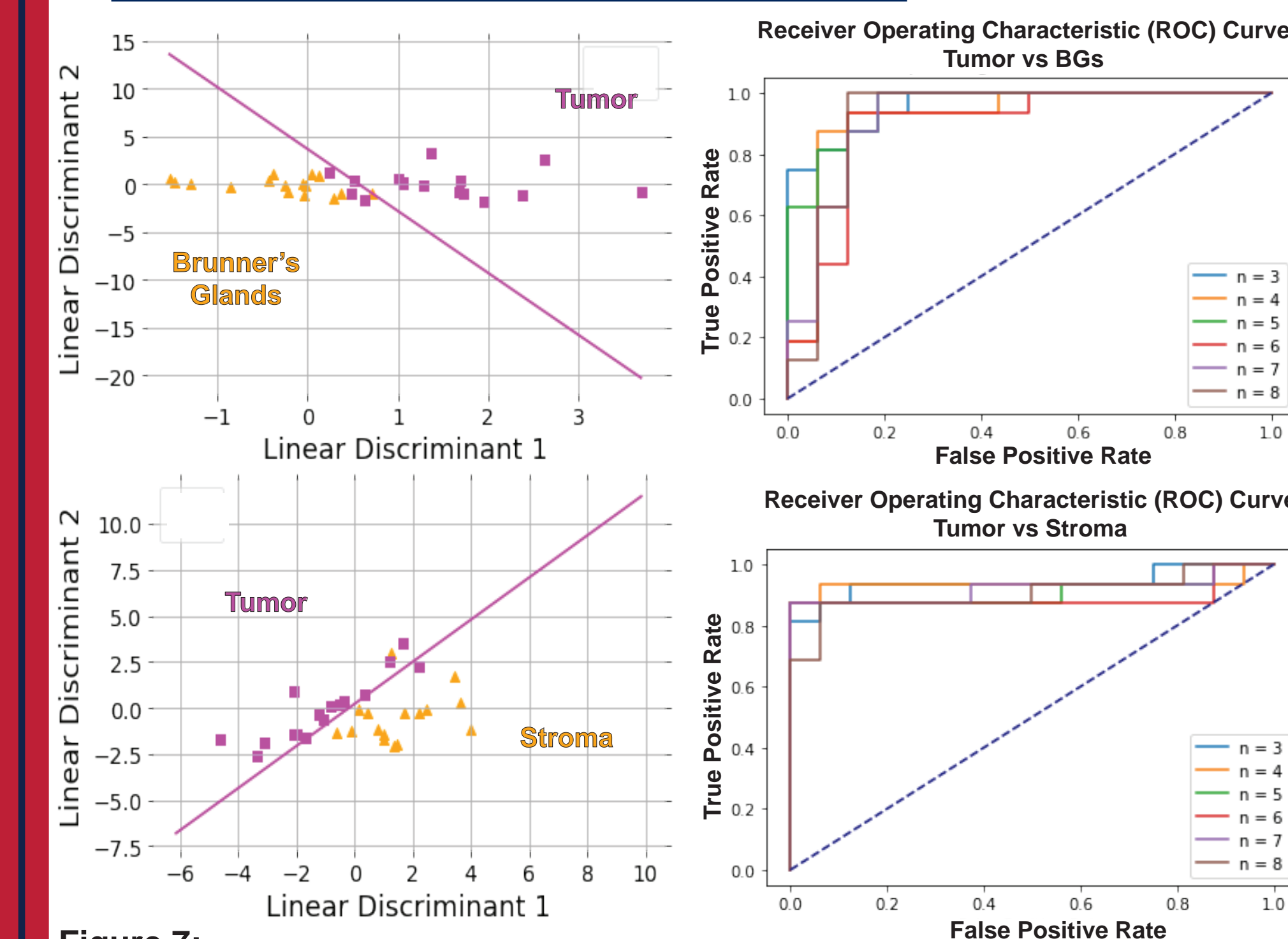
Feature Classification

Figure 7:
Linear discriminant analysis projections and receiver operating characteristic curves for classifiers of the DGast tumors and Brunner's glands (top) and stroma (bottom). n = number of texture features used in the generation of the ROC curve.

Texture features of the 2PEF and SHG image channels were extracted using Haralick's methods[5] and used to create linear discriminant classifiers following principal component analysis with **accuracies ranging from 90 - 96% for distinguishing between tissue types**. Future work will focus on optimizing the generation and performance of these classifiers.

Conclusions

Significant differences in signal intensity of endogenous 2PEF and SHG is measurable in FFPE samples of duodenal gastrinoma using two-photon microscopy. This suggests that MPM can be used as a label-free approach for distinguishing DGasts from normal tissue. Early models using image texture features show high classification accuracy, implying future utility in computer vision-aided diagnostics and potential for detecting early neoplasms with the differentiation between normal/abnormal BGs.

Acknowledgements

References

[1] Norton, J. A. (2005). **Surgical treatment and prognosis of gastrinoma.** Best Practice & Research Clinical Gastroenterology, 19(5), 799–805. https://doi.org/10.1016/J.BPG.2005.05.003
[2] Ragheb, J., Mony, S., Klapman, J., Erim, T., Reagan, A., Butler, R., Dong, Y., Cruise, M., Centeno, B. A., Bejarano, P., Stevens, T., Hayat, U., & Bhatt, A. (2021). Impact of margin status on outcomes after endoscopic resection of well-differentiated duodenal neuroendocrine tumors. Gastrointestinal endoscopy, 94(3), 580–588. https://doi.org/10.1016/j.gie.2021.02.033
[3] Zipfel, W. R., Williams, R. M., Christie, R., Nikitin, A. Y., Hyman, B. T., & Webb, W. W. (2003). **Live Tissue Intrinsic Emission Microscopy Using Multiphoton-Excited Native Fluorescence and Second Harmonic Generation.** Proceedings of the National Academy of Sciences of the United States of America, 100(12), 7075–7080. http://www.jstor.org/stable/3139434
[4] Walsh AJ, Cook RS, Sanders ME, et al. **Quantitative optical imaging of primary tumor organoid metabolism predicts drug response in breast cancer.** Cancer Res. 2014;74(18):5184-5194. doi:10.1158/0008-5472.CAN-14-0663
[5] R. M. Haralick, K. Shanmugam and I. Dinstein, **"Textural Features for Image Classification,"** in IEEE Transactions on Systems, Man, and Cybernetics, vol. SMC-3, no. 6, pp. 610-621, Nov. 1973, doi: 10.1109/TSMC.1973.4309314.
† Imaging Core Marley, University of Arizona